Effects of Heat Treatment on Microstructure and Magnetic Properties of $Fe_{80}Zr_{10}B_{10}$ Alloy

Y.M. Sun*

College of Continuing Education, Jilin Normal University, 1301 Haifeng street, 136000 Siping, China

Received: 31.10.2022 & Accepted: 28.02.2023

Doi: 10.12693/APhysPolA.143.376 *e-mail: sunyaming@jlnu.edu.cn

The metastable crystallization phase of Fe-based alloys remains a popular topic in alloy research. The α-Mn type metastable phase was observed during the crystallization of $Fe_{80}Zr_{10}B_{10}$ amorphous alloy. $Fe_{80}Zr_{10}B_{10}$ amorphous alloy ribbons prepared by melt spinning were annealed at different annealing temperatures and times. Different annealing temperatures indicated that there were large differences in the crystallization phase constitution. Different annealing times indicated that the α-Mn type metastable phase preferentially nucleated relative to the α-Fe phase. A long annealing time resulted in the precipitation of α-Fe and ZrB phases. As the annealing time increased, saturation magnetization (M_s) of the alloy increased gradually (from 75.48 to 122.74 A m^2/kg), and coercivity (H_c) of the alloy increased dramatically (from 0.17 to 15.16 kA/m).

topics: amorphous, heat treatment, saturation magnetization, coercivity

1. Introduction

Amorphous alloys are common thermodynamically metastable materials [1]. After high-pressure, radiation, or high-temperature heat treatment, the amorphous phase tends to transform into a metastable phase or equilibrium phase with lower energy. During the crystallization of the amorphous alloy, the atoms rearrange. To produce a new phase from the amorphous phase, it is necessary to form a nuclear embryo of the new phase. This process requires a large amount of energy. When there is insufficient energy, the process is relatively slow, and a new metastable phase is produced. The precipitation of primary metastable phases during crystallization has been widely reported in Zr-based alloys [2, 3], Mg-based alloys [4], and Al-based alloys [5].

Crystallization of Fe-based amorphous alloys has been an important research topic that has been extensively investigated over the past several decades. Different types of metastable crystallization phases are formed during primary crystallization, such as $Fe_{23}B_6$ type [6–11], α-Mn type (χ) [12–16], cubic quasiperiodic (CQ) [17], $Fe_{12}Si_2ZrB$ type [18, 19], and β-Mn type phases [20–22]. FeZrB system alloys represent an important research direction for Fe-based alloys, and the crystallization phases of FeZrB alloys have been reported in several studies [23–30].

Different heat-treatment conditions can directly affect the composition of the crystallization phases [31–33]. Both the annealing temperature and time are key factors. The research on the crystallization of FeZrB alloy has mostly focused on the effect of heat treatment temperature, and only a few studies have been reported on the effect of annealing time on the crystalline phase of FeZrB amorphous alloys. In this study, the influence of heat treatment conditions (annealing temperature and time) on the microstructural evolution and magnetic properties of $Fe_{80}Zr_{10}B_{10}$ alloy was investigated.

2. Experimental

An ingot of $Fe_{80}Zr_{10}B_{10}$ alloy with nominal composition was prepared by arc melting a mixture of high-purity elements (99.98 wt% Fe, 99.97 wt% Co, 99.92 wt% Zr, 99.99 wt% B). The ingot was remelted four times with magnetic stirring under high-purity argon. Amorphous ribbons were prepared from the ingots by single-roller melt spinning at a copper-wheel rate of 38 m/s and annealed at 500, 600, 700, and 800°C for 20 min in a vacuum. The alloy was also annealed at 600°C for 1, 3, 10, 20, 60, and 120 min.

Structural characterization of the alloys was determined by X-ray diffraction (XRD)(D/Max 2500/PC, Cu K_α, λ = 1.5406 Å) and transmission electron microscopy (TEM)(FEI Talos F200). Magnetic hysteresis loops were measured using a vibrating sample magnetometer (VSM)(Lake Shore M7407).

3. Results and discussion

Figure 1 shows the XRD patterns of the $Fe_{80}Zr_{10}B_{10}$ alloy annealed at different temperatures. No crystalline diffraction peaks were observed for the alloy annealed at 500°C, indicating that the alloy was still in an amorphous state.

When the annealing temperature was 600°C, a metastable α-Mn type (χ) phase and a small amount of α-Fe were observed. The lattice constant of the bcc metastable χ phase is $a = 0.881$ nm, which is close to that of the α-Mn type phase precipitated from $Fe_{80}Nb_{10}B_{10}$ ($a = 0.8846$ nm) [34] and from $Fe_{76}Si_{15}B_6Nb_3$ amorphous alloys ($a = 0.882$ nm) [35]. A further increase in annealing temperature led to the disappearance of the χ-phase and the transformation into both the unknown metastable and the α-Fe phases. When the annealing temperature was 800°C, the metastable unknown phase disappeared, and α-Fe, Fe_3Zr, and other phases were observed. The crystallization was as follows

$$\begin{aligned}&\text{amorphous} \rightarrow \text{residual amorphous}+\chi+\alpha\text{-Fe} \rightarrow \\ &\text{residual amorphous}+\alpha\text{-Fe}+\text{unknown phase} \rightarrow \\ &\alpha-\mathrm{Fe}+\mathrm{Fe_3Zr}+\mathrm{ZrB_2}+\mathrm{ZrFe_2}.\end{aligned} \quad (1)$$

Figure 2 shows the XRD patterns of $Fe_{80}Zr_{10}B_{10}$ alloy annealed at 600°C for different annealing times. When the annealing time was 1 min and 3 min, no crystalline diffraction peaks were observed. When the annealing time was 10 min, the characteristic peaks demonstrated that the α-Mn type phase precipitated from the amorphous matrix, and the primary crystallization phase was only the α-Mn type phase. When the annealing time was 20 min, a small amount of the α-Fe was observed in addition to the α-Mn type phase. With an increase in annealing time, the crystallization volume fraction of α-Fe phase increased. During the crystallization, the α-Mn type phase preferentially

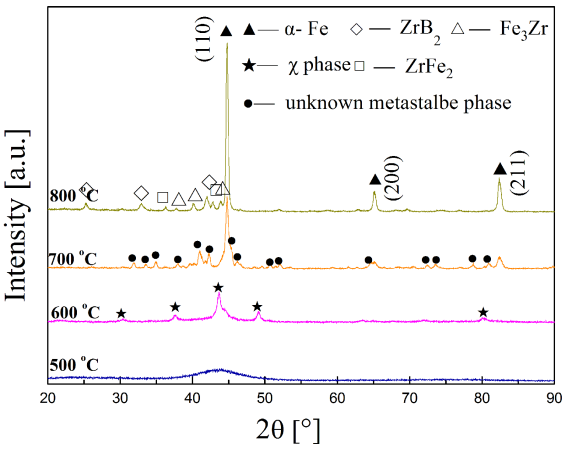

Fig. 1. XRD patterns of $Fe_{80}Zr_{10}B_{10}$ alloy annealed at different temperatures.

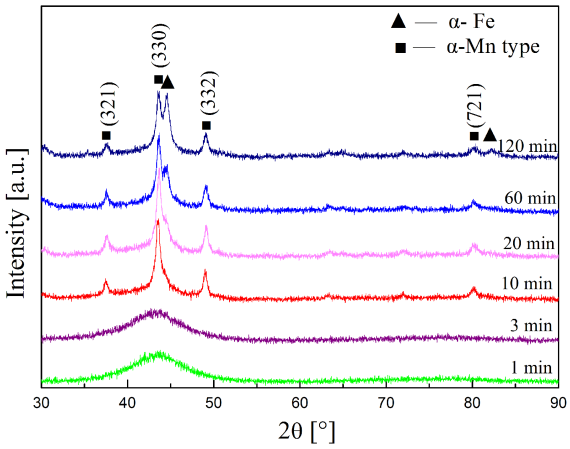

Fig. 2. XRD patterns of $Fe_{80}Zr_{10}B_{10}$ alloy annealed at 600°C for different annealing time.

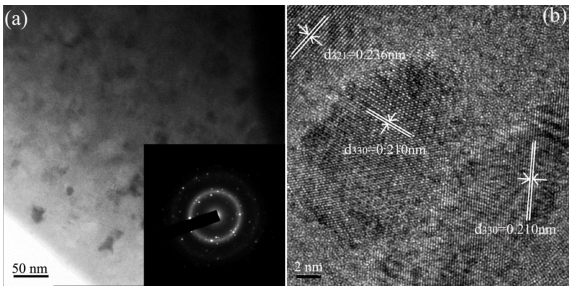

Fig. 3. (a) TEM image and SAED pattern (insert) and (b) HRTEM image of $Fe_{80}Zr_{10}B_{10}$ alloy after annealing at 600°C for 10 min.

nucleated relative to the α-Fe phase. Similar results have been obtained in the previous study [36]. Both stable and metastable phases may precipitate from the amorphous matrix, however, the final crystalline phase depends on the nucleation and growth kinetics of different phases. During the crystallization, the resistance to steady-state crystalline phase precipitation from the amorphous phase is very large, and the alloy system will seek another transformation process with a relatively small transformation resistance. That is, a metastable crystalline phase is formed through non-equilibrium transformation, and the structure of the metastable crystalline phase is relatively close to that of the amorphous parent phase [22]. With the increase of annealing time, α-Mn precipitated to saturation, and then the α-Fe phase precipitated from the remaining amorphous phase.

Figure 3 shows the TEM image, the corresponding selected area electron diffraction (SAED), and high-resolution transmission electron microscopy (HRTEM) image of the alloy annealed at 600°C for 10 min. The irregularly-shaped nanocrystals were surrounded by the remaining amorphous matrix (Fig. 3a). From HRTEM images (Fig. 3b), the calculated d-spacings were 0.236 nm and 0.210 nm,

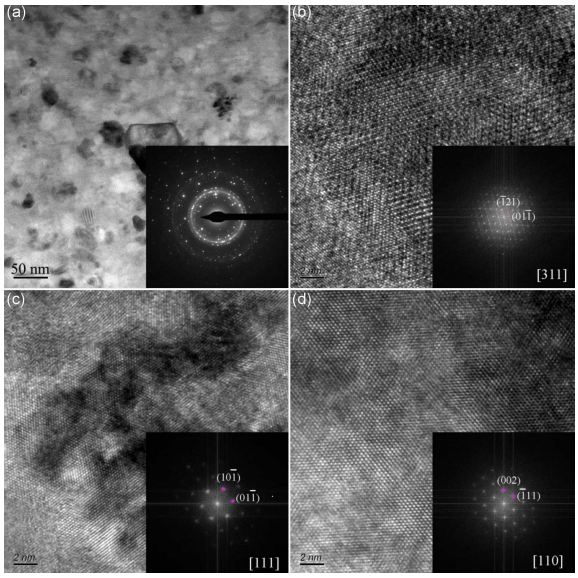

Fig. 4. (a) TEM image and (b–d) HRTEM images of $Fe_{80}Zr_{10}B_{10}$ alloy after annealing at 600°C for 60 min.

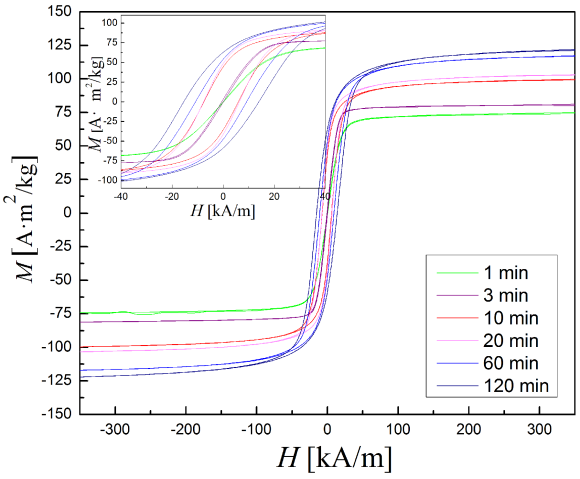

Fig. 5. Magnetic hysteresis loops of $Fe_{80}Zr_{10}B_{10}$ alloy annealed at 600°C for different annealing times.

which correspond to the (321) plane and the (330) plane of the α-Mn type phase, respectively. No other phase was observed. The SAED pattern (insert in Fig. 3a) and HRTEM image (Fig. 3b) showed evidence of only the α-Mn type phase.

Figure 4 shows the TEM (a) and HRTEM (b–d) images of the alloys annealed at 600°C for 60 min. When the annealing time was 60 min (Fig. 4a), many grains of irregular shape were observed that were not uniform in size. The high-resolution image (Fig. 4b–d) and the corresponding diffraction pattern after fast Fourier transform (FFT) conversion (right-hand corner) were shown. Figure 4b indicated that the corresponding grain was an α-Mn type phase grain with a crystal band axis of [311].

TABLE I

Saturation magnetization (M_s) and coercivity (H_c) of $Fe_{80}Zr_{10}B_{10}$ alloy annealed at 600°C for different annealing times.

Time [min]	M_s [A m^2/kg]	H_c [kA/m]
1	75.48	0.17
3	81.40	0.41
10	99.91	6.66
20	101.34	6.94
60	117.46	9.82
120	122.74	15.16

Figure 4c indicated that the corresponding grain was an α-Fe phase grain, and the crystal band axis was [111]. Figure 4d indicated that the corresponding grain was a ZrB phase grain, and the crystal band axis was [110], which was not observed in XRD. Compared with the TEM image of the alloy annealed for 10 min (Fig. 3a), the increase in annealing time significantly increased the size of grains. Furthermore, a long annealing time resulted in the precipitation of α-Fe and ZrB phases.

Figure 5 shows the magnetic hysteresis loops of $Fe_{80}Zr_{10}B_{10}$ alloys annealed at 600°C for different annealing times. The amplification regions of hysteresis loops are shown in the insert. When the annealing times were 1 min and 3 min, the hysteresis loop showed obvious soft magnetic characteristics, which was due to their amorphous structure. With increasing annealing time, the area of the hysteresis loop gradually increased.

Table I lists the values of saturation magnetization (M_s) and coercivity (H_c) of $Fe_{80}Zr_{10}B_{10}$alloys annealed at 600°C for different annealing times. As the annealing time increased, the M_s of the alloy increased gradually (from 75.48 to 122.74 A m^2/kg), and the H_c of the alloy increased dramatically (from 0.17 to 15.16 kA/m). Note that M_s increased gradually due to the increase in the degree of crystallization. When the annealing times were 1 min and 3 min, no crystalline diffraction peaks were observed, and the values of H_c were small. When the annealing times were 10 min and 20 min, almost only the α-Mn type phase precipitated, and the values of H_c significantly increased. When the annealing times were 60 min and 120 min, H_c continued to increase. The value of H_c reached 15.16 kA/m after 120 min.

4. Conclusions

$Fe_{80}Zr_{10}B_{10}$ amorphous alloy ribbons prepared by melt spinning were annealed at different annealing temperatures and times. Both annealing temperature and time have a significant influence on

the structure of the alloy. The crystallization of the $Fe_{80}Zr_{10}B_{10}$ amorphous alloy followed the order shown in (1). Both the α-Mn type (χ) and unknown phase are metastable phases. When the annealing time was 10 min, only the α-Mn type phase existed. With the increase of annealing time, the α-Fe phase precipitated gradually, and the crystallization volume fraction of the α-Fe phase increased. TEM showed that the ZrB phase was also observed at the annealing time of 60 min, along with the α-Mn type and α-Fe phases. With increasing the annealing time, the area of the hysteresis loop gradually increased. Also, M_s of the alloy increased gradually (from 75.48 to 122.74 A m^2/kg), and the H_c of the alloy increased dramatically (from 0.17 to 15.16 kA/m).

Acknowledgments

This work was supported by the Sinoma Institute of Materials Research (Guang Zhou) Co., Ltd and the Natural Science Foundation of Jilin Province (YDZJ202201ZYTS319). We would like to thank Editage for the English language editing.

References

[1] L. Pei, X. Zhang, Z. Yuan, *Metals* **11**, 310 (2021).

[2] A. R. Yavari, A.L. Moulec, A. Inoue, J.B.F. Walter, G. Vaughan, A. Kvick, *Mater. Sci. Eng. A* **304/306**, 34 (2001).

[3] N. Wanderka, M.P. Macht, M. Seidel, S. Mechler, K. Stahl, J.Z. Jiang, *Appl. Phys. Lett.* **77**, 3935 (2000).

[4] V. Angelova, T. Spassov. *J. Alloys Comp.* **345**, 148 (2002).

[5] Y. Liu, W.M. Wang, H.D. Zhang, H.J. Ma, B. An, *J. Mater. Sci. Technol.* **28**, 1102 (2012).

[6] A. Hirata, Y. Hirotsu, K. Amiya, N. Nishiyama, A. Inoue, *Phys. Rev. B* **80**, 140201 (2009).

[7] A. Hirata, Y. Hirotsu, K. Amiya, N. Nishiyama, A. Inoue, *Intermetallics* **16**, 491 (2008).

[8] M. Imafuku, S. Sato, H. Koshiba, E. Matsubara, A. Inoue, *Scr. Mater.* **44**, 2369 (2001).

[9] T.A. Sviridova, T.R. Chueva, M.V. Gorshenkov, E.V. Shelekhov, P.A. Borisova, *J. Alloys Compd.* **658**, 525 (2015).

[10] T. Hibino, T. Bitoh, *J. Alloys Compd.* **707**, 82 (2017).

[11] P. Svec, P. Svec, J. Hosko, D. Janickovic, *J. Alloys Compd.* **590**, 87 (2014).

[12] I.V. Lyasotsky, N.B. Dyakonova, D.L. Dyakonov, *J. Alloys Compd.* **586**, S20 (2014).

[13] T. Nagase, Y. Umakoshi, *Iron Steel Inst. Jpn. Int.* **46**, 1371 (2006).

[14] T.A. Velikanova, M.V. Karpets, *Powder Metal. Metal. Ceram.* **50**, 479 (2011).

[15] Z. Hua, T. Feng, Y. Wu, W. Yu, Y. Liu, *Acta Phys. Pol. A* **141**, 630 (2022).

[16] I.V. Lyasotsky, N.B. Dyakonova, D.L. Dyakonov, V.S. Kraposhin, *J. Phys. Conf. Ser.* **98**, 012026 (2008).

[17] I.V. Lyasotsky, N.B. Dyakonova, D.L. Dyakonov, *J. Alloys Compd.* **586**, S20 (2014).

[18] W.Q. Yu, L.P. Lu, B. Zuo, *Rare Metal Mater. Eng.* **49**, 1561 (2020).

[19] X.Y. Xiong, T.R. Finlayson, B.C. Muddle, *J. Mater. Sci.* **38**, 1161 (2003).

[20] N.B. Dyakonova, D.L. Dyakonov, I.V. Lyasotskyi, *J. Alloys Compd.* **586**, S41 (2014).

[21] J A Loudis, I Baker, *Philos. Mag.* **87**, 5639 (2007).

[22] W.Q. Yu, L.P. Lu, B. Zuo, Z. Hua, G.L. Xing, X.Y. Wang, D.D. Wang, *Appl. Phys. A* **125**, 636 (2019).

[23] W.Q. Yu, L.P. Lu, B. Zuo, *Rare Metal Mater. Eng.* **49**, 1561 (2020).

[24] W.R. Chen, G.H. Tu, *Thermochim. Acta* **333**, 95 (1999).

[25] H. Zheng, L. Zhu, S.S. Jiang, Y.G. Wang, F.G. Chen, *J. Alloys Compd.* **834**,155068 (2020).

[26] T. Tokunaga, K. Terashima, H. Ohtani, M. Hasebe, *Mater. Trans.* **49**, 2534 (2008).

[27] L.H. Kong, Y.L. Gao, T.T. Song, G. Wang, Q.J. Zhai, *Thermochim. Acta* **522**, 166 (2011).

[28] Q.H. Xu, S.S. Jiang, F.G. Chen, A. Jain, Y. Lin, Y.G. Wang, *J. Non-Cryst. Solids* **594**, 121822 (2022).

[29] H. Huang, G. Shao, P. Tsakiropoulos, *J. Alloys Compd.* **459**, 185 (2008).

[30] A. Fernández-Martinez, P. Gorría, G.J. Cuello, J.D. Santos, M.J. Perez, *J. Non-Cryst. Solids* **353**, 855 (2007).

[31] M.J. Duarte, A. Kostka, D. Crespo, J.A. Jimenez, A.C. Dippel, F.U. Renner, G. Dehm, *Acta Mater.*, **127**, 341 (2017).

[32] N.A. Skulkina, O.A. Ivanov, N.D. Denisov, V.I. Chekis, *J. Magn. Magn. Mater.*, **470**, 156 (2019).

[33] L.X. Jiang, Y. Zhang, X. Tong, T. Suzuki, A. Makino, *J. Magn. Magn. Mater.*, **471**, 148 (2019).

[34] M. Imafuku, S. Sato, H. Koshiba, E. Matsubara, A. Inoue, *Mater. Trans.* **41**, 1526 (2000).

[35] I.V. Lyasotskii, N.B. Dyakonova, E.N. Vlasova, D.L. Dyakonov, M.Y. Yazvitskii, *Phys. Status Solidi (a)* **203**, 259 (2006).

[36] Y.M. Sun, B. Zuo, D. Wang, X.C. Meng, J. Liu, L.L. Wang, Z. Hua, *Acta Phys. Pol. A* **124**, 685 (2013).